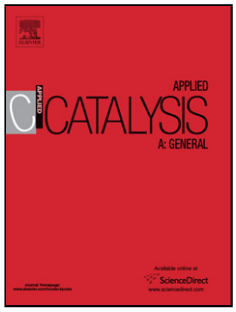

Title: Biomimetic Alkane Oxidation by Iodosylbenzene and Iodobenzene Diacetate Catalyzed by a New Manganese Porphyrin: Water Effect

Author: Vinícius Santos da Silva Ynara Marina Idemori Gilson DeFreitas-Silva

PII: S0926-860X(15)00180-5
DOI: http://dx.doi.org/doi:10.1016/j.apcata.2015.03.022
Reference: APCATA 15312

To appear in: *Applied Catalysis A: General*

Received date: 6-1-2015
Revised date: 16-3-2015
Accepted date: 18-3-2015

Please cite this article as: V.S. Silva, Y.M. Idemori, G. DeFreitas-Silva, Biomimetic Alkane Oxidation by Iodosylbenzene and Iodobenzene Diacetate Catalyzed by a New Manganese Porphyrin: Water Effect, *Applied Catalysis A, General* (2015), http://dx.doi.org/10.1016/j.apcata.2015.03.022

*Graphical Abstract (for review)

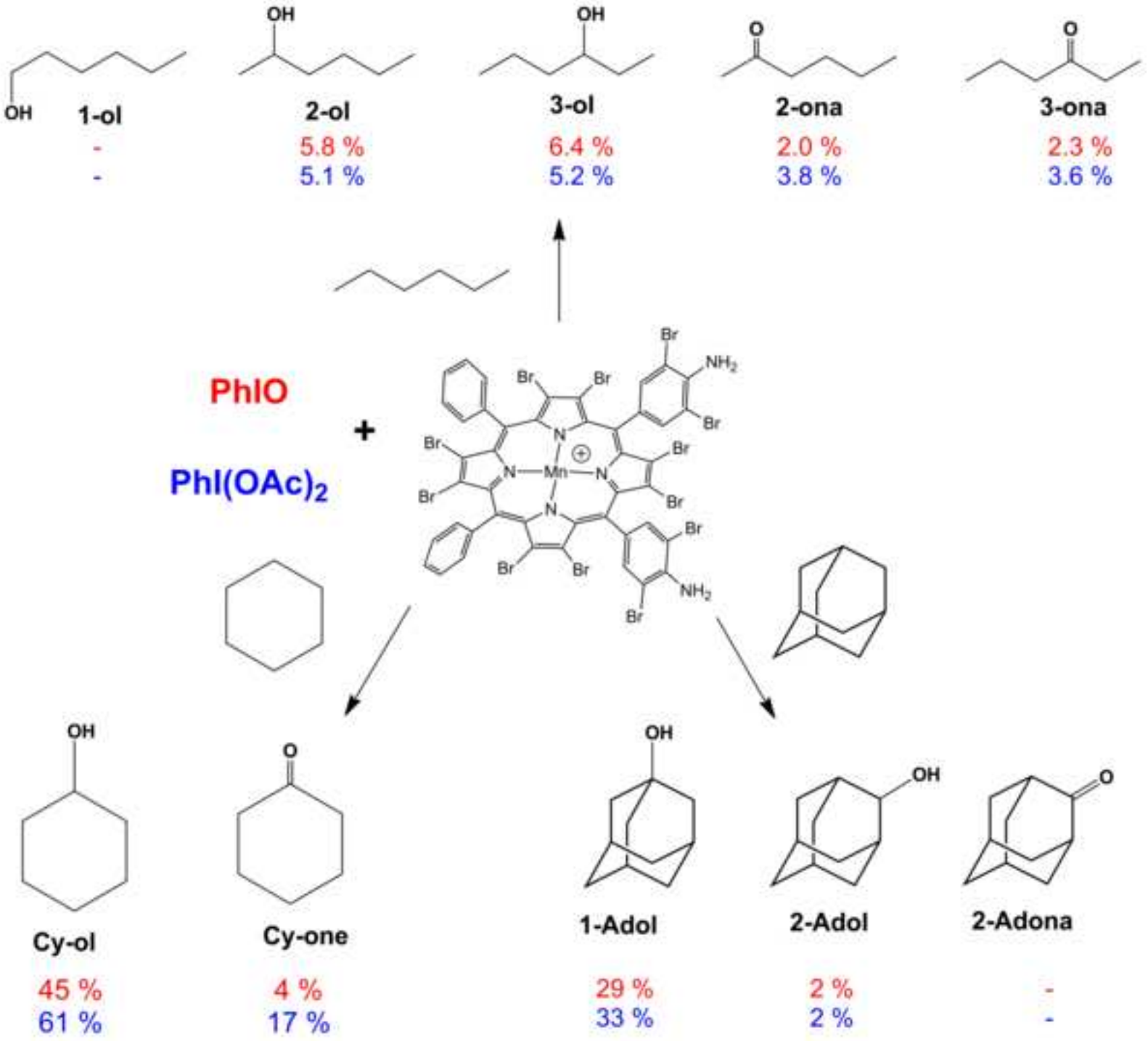

Biomimetic Alkane Oxidation by Iodosylbenzene and Iodobenzene Diacetate Catalyzed by a New Manganese Porphyrin: Water Effect

Highlights

- Synthesis of a novel ß-brominated catalyst derived from a non-symmetric porphyrin.
- Water improve product yield in the cyclohexane oxidation by PhIO or $PhI(OAc)_2$.
- Stability of ß-brominated catalyst toward oxidative degradation in $PhI(OAc)_2$ systems.

Biomimetic Alkane Oxidation by Iodosylbenzene and Iodobenzene Diacetate Catalyzed by a New Manganese Porphyrin: Water Effect

Vinícius Santos da Silva[1], Ynara Marina Idemori[1], Gilson DeFreitas-Silva[1]

*gilsonufmg@ufmg.br

[1] Departamento de Química, Instituto de Ciências Exatas, Universidade Federal de Minas Gerais, 31270-901. Belo Horizonte, MG, Brazil

***Corresponding author:**

Prof. Gilson de Freitas Silva (G. DeFreitas-Silva)

Departamento de Química – Instituto de Ciências Exatas – Universidade Federal de Minas Gerais

Belo Horizonte, MG, 31270-901, BRAZIL

Tel.: +55 31 3409 5772; fax: +55 31 3409 5700.

E-mail address: gilsonufmg@ufmg.br

Abstract: This work describes the synthesis and characterization of the novel third-generation catalyst 5,10-(3,5-bromo,4-aminophenyl)-15,20-(phenyl)-2,3,7,8,12,13,17,18-octabromoporphyrinatomanganese(III) chloride, *cis*-[$Mn^{III}Br_{12}$DAPDPP]Cl, and compares the catalytic activity of this compound with the catalytic activity of the first- and second-generation manganese porphyrins [Mn^{III}TPP]Cl and *cis*-[Mn^{III}DAPDPP]Cl, respectively, in cyclohexane, *n*-hexane, and adamantane oxidation by iodosylbenzene (PhIO) or iodobenzene diacetate ($PhI(OAc)_2$). This work also investigates how addition of water and imidazole influences the catalytic systems in the adamantane and cyclohexane oxidation. In the absence of water and imidazole, *cis*-[$Mn^{III}Br_{12}$DAPDPP]Cl leads to higher product yields as compared with [Mn^{III}TPP]Cl and *cis*-[Mn^{III}DAPDPP]Cl. The third-generation (ß-octabrominated) *cis*-[$Mn^{III}Br_{12}$DAPDPP]Cl was not fully destroyed in reactions with $PhI(OAc)_2$ as oxidant. In the presence of imidazole, [Mn^{III}TPP]Cl and *cis*-[Mn^{III}DAPDPP]Cl give superior cyclohexanol yields as compared with *cis*-[$Mn^{III}Br_{12}$DAPDPP]Cl. Addition of water during adamantane oxidation by $PhI(OAc)_2$ increases 1-adamantanol yield. As for cyclohexane oxidation by PhIO or $PhI(OAc)_2$, the presence of water raises product yields and diminishes catalyst destruction, especially in the case of *cis*-[Mn^{III}DAPDPP]Cl. The presence of water in systems employing $PhI(OAc)_2$ as oxidant affords higher product yields as compared with systems that use PhIO as oxidant.

Keywords: manganese porphyrins; alkanes oxidation; water as additive; iodobenzene diacetate.

1. Introduction

Over the last decades, practical and economic issues have made investigations into the selective oxidation of organic molecules under mild conditions stand out in the scientific field [1]. In this sense, the oxidation of poorly reactive alkanes is noteworthy [2].

Since the work developed by Groves et al. in 1979 [3], when the authors employed a first-generation metalloporphyrin to catalyze alkane hydroxylation and alkene epoxidation, synthetic metalloporphyrins have become the object of many studies on the oxidation of organic substrates by a number of oxygen donors, such as iodosylbenzene (PhIO), periodate (IO_4^-), hypochlorite (ClO^-), and iodobenzene diacetate ($PhI(OAc)_2$) [4, 5]. Despite researchers' efforts, only in 2009 was the first industrial-scale process tested - iron and cobalt porphyrins catalyzed cyclohexane oxidation [6]. Therefore, metalloporphyrin-catalyzed alkane oxidation constitutes a promising area in chemistry, which has stimulated new works with potential future applications.

An interesting strategy to improve the catalytic efficiency of metalloporphyrins is to introduce bulky electron-withdrawing groups into the β-pyrrole positions of the macrocycle. In the particular case of manganese porphyrins (MnP), the substituents make the catalyst more reactive: they destabilize the active species $Mn^V(O)$, which facilitates oxygen atom transfer from this species to the substrate and increases product yield [7-10].

Another approach that enhances catalyst efficiency during MnP-catalyzed oxidation reactions is to add ligands, like imidazole. The ligand influences product yield and selectivity and diminishes catalyst destruction [11, 12] because it can coordinate to the metal ion and weaken the Mn=O bond, making the active species $Mn^V(O)P$ more reactive toward the organic substrate [13]. Moreover, the added ligand can prevent displacement of the metal ion from the porphyrin macrocycle plane, thereby reducing catalyst destruction [11, 13].

Addition of water to such systems can also improve catalyst efficiency; however, there still is no consensus on how water acts during metalloporphyrin-catalyzed biomimetic oxidation. A theoretical study by Barcelles et al. [14] has shown that water may act as an axial ligand. On the other hand, In et al. [15] have reported that water hydrolyzes $PhI(OAc)_2$, to generate PhIO in situ. Silva et al. [16] have verified that water enhances catalyst efficiency during cyclohexane oxidation by PhIO and $PhI(OAc)_2$, whereas CarvalhoDa-Silva et al. [17] have not detected any rise in product yield upon addition of water to systems that employ PhIO as oxidant.

In this context, we have synthesized and characterized a novel β-octabrominated MnP, 5,10-(3,5-bromo-4-aminophenyl)-15,20-(phenyl)-2,3,7,8,12,13,17,18-octabromoporphyrinatomanganese(III) chloride (cis-[$Mn^{III}Br_{12}$DAPDPP]Cl, Figure 1) derived from 5,10-(4-aminophenyl)-15,20-(phenyl)porphyrin (cis-H_2DAPDPP, Figure 1) and applied it as a biomimetic catalyst. We used *cis*-[$Mn^{III}Br_{12}$DAPDPP]Cl and its non-brominated counterpart *cis*-[Mn^{III}DAPDPP]Cl (Figure 1) in alkane (cyclohexane, adamantane, or *n*-hexane) oxidation by iodosylbenzene (PhIO) or iodobenzene diacetate ($PhI(OAc)_2$). Knowing that addition of ligands to the reaction medium significantly improves the catalytic efficiency of MnPs [28, 31, 33], we also conducted oxidation reactions in the presence of imidazole or water, to verify how they affect the oxidative process.

Figure 1

2. Experimental

2.1. Materials and Methods

2.1.1. Reagents

5,10,15,20-tetraphenylporphyrin (H_2TPP, Figure 1) was purchased from Aldrich Chemical Co and was purified on an alumina column; CH_2Cl_2 was used as solvent. H_2TPP: UV–vis ($CHCl_3$), λ_{max}, nm (log ε): 421 (5.48), 516 (4.13), 551 (3.92), 591 (3.81),

and 645 (3.74) [17]. The first-generation MnP complex [Mn^{III}TPP]Cl (Figure 1) was synthesized as reported in the literature [18]: UV–vis (CH_3CN), λ_{max} (nm), (log ε): 373 (4.65), 400 (4.57), 475 (4.96), 528 (3.64), 581 (3.87), 618 (3.96), 763 (2.56). Analytical grade CH_3CN, CH_3OH, CH_2Cl_2, N,N-dimethylformamide (DMF), and $CHCl_3$ were obtained from Aldrich Chemical Co and distilled prior to use. PhIO was prepared according to a literature procedure [19], stored at −20° C in a freezer, and assayed periodically by iodometric titrations. All the other reagents and solvents were of analytical grade and were used without further purification, unless stated otherwise.

2.1.2. Equipment

UV–vis spectra (190–1100 nm) were recorded on an HP-8453A diode-array spectrophotometer. Infrared (IR) spectra were registered on a Perkin Elmer spectrometer model BXFTIR; the samples were prepared in KBr pellets. Room-temperature (25 °C) ^{1}H NMR spectra were obtained in $CDCl_3$ on a Bruker DPX-200 Advance spectrometer operating at 200 MHz; tetramethylsilane (TMS) was the internal standard. Gas chromatography was conducted on a Shimadzu GC-17A chromatograph equipped with a flame ionization detector and a Carbowax capillary column (measuring 30.0 m × 0.32 mm, with a film thickness of 0.25 μm). The ultrasound equipment Unique® MaxiClean 1400, 40 kHz, was also employed in the experiments. Cyclic voltammetry was carried out on an Eco Chemie l-Autolab potentiostat; the GPES software was used. The electrochemical cell contained a homemade glassy carbon working electrode, a platinum wire counter electrode, and a homemade Ag/AgCl reference electrode. Before each measurement, the working electrode surface was polished to a mirror finish with alumina, rinsed thoroughly with water, cleaned in an ultrasonic bath with water, and rinsed with water and ethanol. The electrochemical measurements were accomplished under N_2 in dry CH_2Cl_2 solutions containing 0.1 mol L^{-1} N-tetrabutylammonium tetrafluoroborate ($TBABF_4$, Aldrich, 99%) as supporting electrolyte, MnP 0.5 mmol L^{-1}, and ferrocene as internal standard. Half-wave potentials

($E_{1/2}$) are reported versus the Fc^+/Fc couple, as recommended by IUPAC for measurements in non-aqueous solvents [20]. Three to five voltammograms were run for each manganese porphyrin at any given scan rate (10, 25, 50, 100, 200, and 500 mV s^{-1}). The ESI-MS analyses were conducted on an LCQFleet (ThermoScientific, San Jose, CA, USA) mass spectrometer equipped with electrospray ionization (ESI) source operating in the positive ion mode; CH_3OH was used as solvent.

2.2. Metalloporphyrin catalyst synthesis

2.2.1. 5,10-(4-nitrophenyl)-15,20-diphenylporphyrin – cis-H_2DNPDPP and 5,15-(4-nitrophenyl)-10,20-diphenylporphyrin – trans-H_2DNPDPP

The *cis/trans-H_2DNPDPP* isomers originated as byproducts of H_2TPP nitration [16]. The isomers mixture was purified by liquid chromatography on silica (Sigma-Aldrich, 130-270 mesh) column with $CHCl_3$ as eluent. UV-vis electron absorption spectroscopy, infrared vibrational spectroscopy, and ^{1}H NMR aided product characterization.

2.2.2. 5,10-(4-aminophenyl)-15,20-diphenylporphyrin – cis-H_2DAPDPP and 5,15-(4-aminophenyl)-10,20-diphenylporphyrin – trans-H_2DAPDPP

The mixture containing the dinitrophenylporphyrin isomers (*cis- and trans*-H_2DNPDPP, 198.08 mg, 0.28111 mmol) resulting from H_2TPP nitration was reduced according to an adaptation of the procedure proposed by Hasegawa et al. [21]. Concentrated hydrochloric acid (20 mL) and tin(II) chloride dihydrate (368.18 mg, 1.6318 mmol) were used in the process, to afford *cis*-H_2DAPDPP and *trans*-H_2DAPDPP. These porphyrins were purified by liquid chromatography on silica (Sigma-Aldrich, 130-270 mesh) column; $CHCl_3$ was the eluent. This procedure separated the dinitrophenylporphyrins *cis*- and *trans*-H_2DNPDPP, which eluted first, from the diaminophenylporphyrins *cis*- and *trans*-H_2DAPDPP. The fractions corresponding to the aminophenylporphyrins were dried in the rotary evaporator. The mixture of *cis*- and *trans*-H_2DAPDPP isomers was solubilized in a small chloroform volume and separated by thin layer chromatography

(TLC) on silica (Sigma-Aldrich, 2-25 µm) as the stationary phase. The TLC plate was 0.5 mm thick, 22 cm high, and 20 cm large. The solution containing the mixture of porphyrins (70 µL) was applied on the TLC plate and eluted with a chloroform/hexane/ethyl acetate (2:1:1) mixture. The fractions corresponding to the *cis*- (Rf. 0.21) and *trans*- (Rf. 0.43) isomers were removed with a spatula. The silica/porphyrin fractions of each isomer were extracted with $CHCl_3$, which was then removed in the rotary evaporator. The product was placed in a desiccator containing SiO_2. UV-vis electron absorption spectroscopy, infrared vibrational spectroscopy, and ^{1}H NMR aided characterization of the porphyrins.

Reaction yield: *trans*-H_2DAPDPP: 21.40 mg, 0.03319 mmol, 12 %.

UV–vis ($CHCl_3$) λ_{max}, nm (log ε): 424 (5.25), 522 (4.16), 557 (4.05), 594 (3.78), and 650 (3.71). ^{1}H NMR $CDCl_3$ δ: 8.95 (m, 4H), 8.85 (m, 4H), 8.24 (m, 4H), 8.03 (s, 4H), 7.78 (m, 6H), 7.10 (m, 4H), 4.05 (4H), and -2.73 (s, 2 H).

Reaction yield: *cis*-H_2DAPDPP: 100.86 mg, 0.15643 mmol, 56 %.

UV–vis ($CHCl_3$) λ_{max}, nm (log ε): 423 (5.44), 520 (4.13), 557 (3.98), 593 (3.63), and 650 (3.66). ^{1}H NMR $CDCl_3$ δ: 8.94 (s, 4H), 8.83 (s, 4H), 8.24 (m, 4H), 8.03 (s, 4H), 7.78 (m, 6H), 7.10 (m, 4H), 4.04 (4H), and -2.73 (s, 2 H).

2.2.3. 5,10-(4-aminophenyl)-15,20-(phenyl)porphyrinatomanganese(III) chloride (cis-[Mn^{III}DAPDPP]Cl)

The metalloporphyrin *cis*-[Mn^{III}DAPDPP]Cl (Figure 1) was obtained according to the protocol described by Silva et al. [16], which employed the free-base porphyrin (30.51 mg, 0.04732 mmol) and $Mn(OAc)_2.4H_2O$ (125 mg). Yield 88 % (30.66 mg, 0.04182 mmol). UV–vis ($CHCl_3$), λ_{max} (nm) (log ε): 381(4.25), 481(4.56), 586(3.56), and 624(3.70). FTIR in KBr pellets (cm^{-1}): (1620) δ NH_2, (1294) δ porphyrin skeleton, (1010) δ Mn-N. ESI-MS in CH_3OH [*cis*-Mn^{III}DAPDPP]$^+$ *m/z* (relative intensity) 697 (100 %).

2.2.4. 5,10-(3,5-bromo-4-aminophenyl)-15,20- (phenyl)-2,3,7,8,12,13,17,18-octabromo-porphyrinatomanganese(III) chloride (cis-[$Mn^{III}Br_{12}$DAPDPP]Cl)

The metalloporphyrin *cis*-[$Mn^{III}Br_{12}$DAPDPP]Cl (Figure 1) was synthesized as described by Silva et al. [16]; *cis*-[Mn^{III}DAPDPP]Cl (25.75 mg, 0.03512 mmol) and liquid bromine (~0.3 mL, 5.4 mmol, 100-fold molar excess) were employed. The reaction lasted 1 h. The yield was 64 % (37.64 mg, 0.02241 mmol). UV–vis ($CHCl_3$), λ_{max} (nm) (log ε): 394 (4.64), 508 (4.85), 622 (3.98), and 664 (4.08). FTIR in KBr (cm^{-1}): (1313) δ porphyrin skeleton, (1227) ν Cβ-Br, (1042) δ Mn-N. ESI-MS in the positive mode, in CH_3OH: *cis*-[$Mn^{III}Br_{12}$DAPDPP - Cl^-] *m/z* (relative intensity) 1644 (56%); *cis*-[$Mn^{III}Br_{12}$DAPDPP – Br^- and Cl^-] *m/z* (relative intensity) 1566.2 (97.2%), *cis*-[$Mn^{III}Br_{12}$DAPDPP – 2 Br^- and Cl^-] *m/z* (relative intensity) 1486.3 (100%)

2.3. Alkane oxidation reactions

All the catalytic reactions were performed in 2-mL Wheaton® vials sealed with teflon-faced silicon septa. Reactions were conducted under magnetic stirring, at 25 ℃, for 90 min, according to procedures adapted from de Sousa et al. [22]. Oxidation was carried out in air; either $PhI(OAc)_2$ or PhIO was used as oxygen donor. Reaction mixtures comprised 2.0×10^{-4} mmol of the catalyst (MnP); 2.0×10^{-3} mmol of the oxidant (PhIO or $PhI(OAc)_2$); 100 µL of cyclohexane (0.93 mmol), or 100 µL of *n*-hexane (0.76 mmol), or 100 µL of adamantane solution in CH_2Cl_2 (0.2 mol L^{-1}; 0.02 mmol); and 200 µL of CH_2Cl_2. The catalyst/oxidant/substrate molar ratio was 1:10:4650 for cyclohexane, and 1:10:3800 for *n*-hexane. As for adamantane, the catalyst/oxidant/substrate molar ratio was 1:10:100, because adamantane was poorly soluble in CH_2Cl_2. When deemed necessary, the reaction was quenched by addition of sulfite and borax solution [22]. The reaction mixtures were analyzed by capillary gas chromatography; bromobenzene was the internal standard. The retention times of the products were confirmed by comparison with the retention times of authentic product samples [23]. The yields were based on either initial PhIO or $PhI(OAc)_2$. Each reaction was accomplished at least

three times, and the reported data represent the average of the results of these reactions. Errors in yields and selectivity were calculated on the basis of the reproducibility of the reactions. The degree of MnP destruction (bleaching) was determined by UV–vis spectroscopy at the end of the catalytic run. Control reactions were conducted in the absence of the catalyst. The effect of imidazole was studied by adding a 10-µL aliquot of an imidazole (Im) 1.0×10^{-2} M solution in CH_2Cl_2 to the reaction medium. To test the effect of water on adamantane oxidation, 0.5 µL of water was added to the reaction mixture. As for cyclohexane oxidation, different volumes of water were added - 0.5 µL, 1.0 µL, 2.5 µL, and 5.0 µL.

3. Results and Discussion

3.1. Synthesis

The method proposed by Luguya et al. [24] leads to low H_2NPTPP yields. Nevertheless, the mixture of *cis*- and *trans*-H_2DNPDPP isomers is the main product, and reduction of these isomers affords the diaminophenylporphyrins *cis*- and *trans*-H_2DAPDPP.

The UV-vis spectra of the *cis*- and *trans*-isomers (Supplementary material) agree with literature data [24] and are not significantly different. The spectral profile results from the presence of an amino group (-NH_2) at two *para*-*meso*aryl positions of the macrocycle. Because these groups and the porphyrin macrocycle are arranged in different planes, steric hindrance prevents them from interacting with the π-electron cloud of the porphyrin ring [25].

The vibrational spectra (Supplementary Material) indicate reduction of the nitro group to amino - the band at 1620 cm^{-1} refers to symmetric angular deformation of the plane corresponding to the amino group N-H bond.

The methodology described by Silva et al. [16] yields the second-generation *cis*-[Mn^{III}DAPDPP]Cl and the third-generation *cis*-[$Mn^{III}Br_{12}$DAPDPP]Cl. UV-vis absorption

spectroscopy, infrared vibrational spectroscopy, and mass spectrometry aided characterization of these metalloporphyrins.

The UV-vis spectra (Figure 2) confirm metal insertion into the porphyrin ring. The spectra of the MnP display an LMCT band at 385 nm, typical of these complexes, and fewer bands in the visible region. The infrared vibrational spectra attest to metal insertion into the porphyrin ring, too - the band due to N-H (pyrrole) bond deformation is absent, and a new band due to axial deformation of the Mn-$N_{pyrrole}$ bond arises [26].

Figure 2

UV-vis spectroscopy helped to monitor the bromination reaction. Macrocycle polybromination occurs within only one hour. This result suggests that the presence of the amino group, which donates electron density, increases the reactivity of the β-pyrrole and *ortho-meso*aryl positions of the macrocycle. Figure 2 reveals a bathochromic shift in the Soret band of *cis*-[$Mn^{III}Br_{12}$DAPDPP]Cl as compared with the Soret band of *cis*-[Mn^{III}DAPDPP]Cl. This shift usually occurs upon bromination of MnP, as discussed in the literature [17, 27-29].

The mass spectra of *cis*-[Mn^{III}DAPDPP]Cl and *cis*-[$Mn^{III}Br_{12}$DAPDPP]Cl (Supplementary Material) present a peak at *m/z* 697.2 and 1644.1, respectively, associated with loss of the chloride ion. The fact that the amino groups activate and drive substitutions at the *ortho*- and *para-meso*aryl positions of the porphyrin macrocycle justifies the introduction of bromine atoms into the *meso*aryl rings. Because the *para-meso*aryl position relative to the amino substituent contain the porphyrin macrocycle, substitutions with bromine only occur in the *ortho-meso*aryl positions relative to $–NH_2$.

3.2. Electrochemistry

The redox potentials associated with the macrocycle and the metal center directly affect formation of the high-valent catalytically active species that oxidizes organic substrates [30].

Table 1 contains the data relative to the redox process centered on the metal ion (Mn^{III} + e^{-} ⇌ Mn^{II}). The studied systems are quasi-reversible, because they do not obey some of the typical reversibility parameters described by Matsuda and Ayabe [52]. The Mn^{III}/Mn^{II} reduction potential of *cis*-[$Mn^{III}Br_{12}$DAPDPP]Cl undergoes a 506-mV anodic shift as compared with *cis*-[Mn^{III}DAPDPP]Cl – the bromine atoms withdraw electron density from the macrocycle and the metal center, thereby stabilizing the energy of the frontier orbitals HOMO and LUMO and favoring metal reduction [31, 32]. Additionally, the steric hindrance conferred by bromine distorts the macrocycle and destabilizes the energy levels of the HOMO, but not of the LUMO orbitals. The difference between the energies of the HOMO and LUMO orbitals decreases, culminating in the anodic shift of the metal center redox potential [28, 33].

Table 1

3.3. Catalytic studies

Investigation into the oxidation of poorly reactive substrates such as cyclohexane, *n*-hexane and adamantane (Fig. 3) enables comparison of catalyst efficiency during oxidation of linear and cyclic alkanes [5].

This work used two distinct oxygen donors in the MnP-catalyzed alkane oxidation reactions: PhIO and $PhI(OAc)_2$. It also examined how addition of water and imidazole affects cyclohexane and adamantane oxidation.

Figure 3

3.3.1. MnP-catalyzed n-Hexane oxidation by PhIO or PhI(OAc)$_2$

Linear alkane oxidation is a highly complex process. For this reason, this chemical transformation has attracted the attention of the scientific community [5, 34, 35]. Because the literature contains few papers on metalloporphyrin-catalyzed *n*-hexane oxidation [36, 37], this work aimed to evaluate the efficiency of the synthesized MnP catalysts in the oxidation of *n*-hexane by PhIO and PhI(OAc)$_2$.

Fig. 4 reveals that the second-generation *cis*-[Mn^{III}DAPDPP]Cl catalyzes *n*-hexane oxidation by PhIO less efficiently than the third-generation *cis*-[Mn^{III}Br$_{12}$DAPDPP]Cl, as judged from the product yields. Moreover, *cis*-[Mn^{III}DAPDPP]Cl undergoes more extensive degradation as compared with *cis*-[Mn^{III}Br$_{12}$DAPDPP]Cl, which is also true when PhI(OAc)$_2$ is the oxidant. Comparison between the systems that use PhIO and PhI(OAc)$_2$ shows that the oxidation product yields remain virtually the same in the case of *cis*-[Mn^{III}DAPDPP]Cl, but PhI(OAc)$_2$ destroys the catalyst to a larger extent. As for *cis*-[Mn^{III}Br$_{12}$DAPDPP]Cl, product yields are slightly better when PhI(OAc)$_2$ is the oxidant.

Figure 4

An interesting aspect of linear alkane oxidation is selectivity in terms of the oxidation of primary, secondary, and tertiary carbons, which present distinct bond dissociation energies: 435.4, 396.1, and 391.1 kJ mol^{-1}, respectively [38]. These energies explain why none of the reactions afford 1-hexanol; they are also the reason why 3-hexanol is the preferential product.

The third-generation *cis*-[Mn^{III}Br$_{12}$DAPDPP]Cl gives the highest 2-ol/3-ol ratio. The use of PhI(OAc)$_2$ as oxidant results in 2-ol/3-ol ratios of ~1. Comparison between alcohol and ketone product yields reveals that the MnPs are more selective for alcohol products when PhIO is the oxidant. Because MnP-catalyzed *n*-hexane oxidation affords

low product yields, we decide to not evaluate the effects of water and imidazole addition to the catalytic systems.

3.3.2. MnP-catalyzed adamantane oxidation by PhIO

Adamantane is a cyclic alkane that is more reactive than linear alkanes. It can undergo oxidation at the tertiary carbon, to give 1-adamantanol (1-Adol), or at the secondary carbon, to furnish 2-adamantanol (2-Adol) and 2-adamantanone (2-Adone). Fig. 5 summarizes the results from adamantane oxidation catalyzed by *cis*-[Mn^{III}DAPDPP]Cl and *cis*-[$Mn^{III}Br_{12}$DAPDPP]Cl.

Figure 5

As in the case of *n*-hexane, the third-generation *cis*-[$Mn^{III}Br_{12}$DAPDPP]Cl catalyzes adamantane oxidation more efficiently than the second-generation *cis*-[Mn^{III}DAPDPP]Cl, providing larger 1-Adol and 2-Adol yields as well as lower degree of catalyst destruction. Both *cis*-[Mn^{III}DAPDPP]Cl and *cis*-[$Mn^{III}Br_{12}$DAPDPP]Cl are over 95 % regioselective for 1-Adol. The ketone product (2-Adone) emerges in smaller amounts (~ 0.5 %).

Comparison of the efficiency of the MnPs prepared herein with the efficiency of some catalysts described in the literature shows that the second-generation *cis*-[Mn^{III}DAPDPP]Cl leads to product yields similar to those reported by Groves et al. [3], whereas the third-generation *cis*-[$Mn^{III}Br_{12}$DAPDPP]Cl is more efficient. In the latter case, the bromine atoms introduced into the β-pyrrole positions of the porphyrin ring withdraw electron density from the metal center, to destabilize the high-valent active species. In addition, these same bromine atoms distort the metalloporphyrin macrocycle, which acquires a saddle-type conformation [39] that diminishes self-oxidation and consequent catalyst degradation [9, 17, 33]. However, comparison of the efficiency of the second-generation *cis*-[Mn^{III}DAPDPP]Cl with the efficiency of the

second-generation [Mn^{III}(PFTDCPP)]Cl obtained by Doro et al. [40] demonstrates that the latter catalyst is much more efficient. This might be associated with the presence of electron-withdrawing substituents (fluorine and chlorine) in the *ortho*-, *meta*-, and *para-meso*aryl positions of the porphyrin ring in [Mn^{III}(PFTDCPP)]Cl, which make the high-valent active species more reactive and less prone to self-oxidation [4]. Besides that, Doro et al. [40] used a much higher MnP/PhIO ratio (1:100) than the one employed herein (1:10).

Addition of imidazole to the system based on [Mn^{III}DAPDPP]Cl almost does not alter 1-Adol and 2-Adol yields, but it decreases catalyst degradation. Doro et al. [40] reported similar results for a higher MnP/Im molar ratio (1:20 versus 1:0.5 in our case). As for the third-generation *cis*-[$Mn^{III}Br_{12}$DAPDPP]Cl, the 1-Adol yield drops slightly, and addition of imidazole does not change the degree of catalyst destruction. When Doro et al. [40] used the third-generation [Mn^{II}(PFTDCCl_8PP)] to catalyze adamantane oxidation by PhIO in the presence of imidazole, they achieved superior yields of hydroxylated products as compared with *cis*-[$Mn^{III}Br_{12}$DAPDPP]Cl. This difference may be associated with the MnP/Im molar ratio: Doro et al. [40] used 1:30, whilst in this work the ratio is 1:0.5. Moreover, [Mn^{II}(PFTDCCl_8PP)] bears electron-withdrawing substituents (Cl and F) in the *ortho*-, *meta*-, and *para-meso*aryl positions of the porphyrin macrocycle, which enhance the reactivity of the high-valent active species.

Addition of water diminishes product yields for both the second-generation *cis*-[Mn^{III}DAPDPP]Cl and the third-generation *cis*-[$Mn^{III}Br_{12}$DAPDPP]Cl, but catalyst degradation decreases in the former case. The lesser degradation of *cis*-[Mn^{III}DAPDPP]Cl might stem from water coordination to the metal center, which prevents displacement of the metal ion from the porphyrin macrocycle and avoids catalyst self-oxidation.

3.3.3. MnP-catalyzed adamantane oxidation by PhI(OAc)$_2$

$PhI(OAc)_2$ constitutes an alternative to PhIO. During MnP-catalyzed adamantane oxidation by $PhI(OAc)_2$, the second-generation *cis*-[Mn^{III}DAPDPP]Cl affords lower 1-Adol yield and catalyst degradation is higher as compared with the third-generation *cis*-[$Mn^{III}Br_{12}$DAPDPP]Cl. Interestingly, despite the smaller product yield, *cis*-[Mn^{III}DAPDPP]Cl does not generate 2-Adol, which makes the system 100% regioselective. Comparison between $PhI(OAc)_2$ and PhIO reveals that *cis*-[Mn^{III}DAPDPP]Cl yields less 1-Adol and undergoes more extensive destruction in the presence of the former oxidant. Nevertheless, the system is 100% regioselective for 1-Adol. Regarding *cis*-[$Mn^{III}Br_{12}$DAPDPP]Cl, $PhI(OAc)_2$ gives better product yields as compared with PhIO. Li and Xia [41] have already reported on the use of $PhI(OAc)_2$ to oxidize adamantane in the presence of MnPs. These authors achieved 32 and 1 % yield of 1-Adol and 2-Adol, respectively, when they employed [Mn^{III}TPP]Cl as catalyst in the presence of ionic liquids. Their results resembled the results obtained for *cis*-[$Mn^{III}Br_{12}$DAPDPP]Cl. It is noteworthy that Li and Xia used a MnP/$PhI(OAc)_2$ ratio of 1:225 versus the MnP/$PhI(OAc)_2$ ratio of 1:10 employed here. When these authors used the second-generation [$Mn^{III}TPPS_4$], the 1-Adol and 2-Adol yields were 52 and 2%, respectively [41].

Addition of imidazole to the catalytic systems at a MnP/Imidazole ratio of 1:0.5 does not alter 1-Adol yields in the case of the second-generation *cis*-[Mn^{III}DAPDPP]Cl, but catalyst destruction increases. As for the third-generation *cis*-[$Mn^{III}Br_{12}$DAPDPP]Cl, addition of imidazole does not augment the 1-Adol yield. Therefore, the use of imidazole at a MnP/Imidazole ratio of 1:0.5 is not advantageous in these systems. Li and Xia [41] added imidazole to adamantane oxidation reactions by $PhI(OAc)_2$ catalyzed by the first-generation [Mn^{III}TPP]Cl and the second-generation [$Mn^{III}TPPS_4$] in ionic liquids. They verified that 1-Adol yields increased at a MnP/Imidazole ratio of 1:50. We believe that the MnP/Im ratio used herein is low, so further studies are necessary to obtain more efficient catalytic systems.

Addition of water to the systems that use $PhI(OAc)_2$ as oxidant raises 1-Adol yields slightly for both *cis*-[Mn^{III}DAPDPP]Cl and *cis*-[$Mn^{III}Br_{12}$DAPDPP]Cl. These results reinforce the proposal of In et al., who suggested that $PhI(OAc)_2$ hydrolysis generates PhIO in situ [15]. On the other hand, addition of water to the systems in which PhIO is the oxidant affects the yield of hydroxylated products very little.

3.3.4. MnP-catalyzed cyclohexane oxidation by PhIO

Cyclohexanol (Cy-ol) and cyclohexanone (Cy-one) are the main products of cyclohexane oxidation catalyzed by the investigated MnPs. Fig. 6 shows that, when PhIO is the oxidant, the second-generation *cis*-[Mn^{III}DAPDPP]Cl gives better results and is more selective toward Cy-ol as compared with the first-generation [Mn^{III}TPP]Cl. This result is probably associated with the presence of the amino group in the *para*-mesoaryl positions of the porphyrin macrocycle - this group may coordinate to the metal center of another MnP, to destabilize the high-valent Mn^{V}(O)P species and make it more reactive [16, 42, 43].

The system based on the third-generation *cis*-[$Mn^{III}Br_{12}$DAPDPP]Cl is extremely selective and affords significantly higher Cy-ol yield as compared with the systems based on the first-generation [Mn^{III}TPP]Cl and on the second-generation *cis*-[Mn^{III}DAPDPP]Cl. This evidences the importance of introducing bromine substituents into the β-pyrrole positions of the porphyrin macrocycle.

Figure 6

The results depicted in Fig. 6 show that addition of imidazole to the system based on the [Mn^{II}TPP]Cl significantly improves product yield and selectivity toward Cy-ol, which agrees with literature reports [16, 22]. Indeed, imidazole can coordinate to the metal ion and weaken the Mn=O bond, making the active species Mn^{V}(O)P more reactive toward the organic substrate. As for *cis*-[Mn^{III}DAPDPP]Cl, addition of imidazole does not affect

product yield significantly, because the amino group in the MnP may coordinate to the metal center of another MnP and diminish the effects of imidazole [43].

Addition of imidazole at a MnP/Im 1:0.5 ratio to the system based on the third-generation *cis*-[$Mn^{III}Br_{12}$DAPDPP]Cl reduces product yield. Repulsive interactions between the pentacoordinated MnP (MnP + imidazole and/or MnP + MnP) and the oxidant PhIO might take place, because the saddle-shaped β-octabrominated porphyrin macrocycle [39] favors repulsion between the bromine atoms and PhIO. As a consequence, formation of the high-valent active species becomes more difficult.

3.3.5. MnP-catalyzed cyclohexane oxidation by PhI(OAc)$_2$

Comparison of the efficiency of [Mn^{III}TPP]Cl, *cis*-[Mn^{III}DAPDPP]Cl, and *cis*-[$Mn^{III}Br_{12}$DAPDPP]Cl in cyclohexane oxidation by PhI(OAc)$_2$ reveals that *cis*-[$Mn^{III}Br_{12}$DAPDPP]Cl is the most efficient, but this third-generation catalyst is less resistant to self-oxidation. Comparison between the oxidants PhIO and PhI(OAc)$_2$ shows that the product yields vary very little when [Mn^{III}TPP]Cl and *cis*-[Mn^{III}DAPDPP]Cl are the catalysts. In turn, the yields markedly increase in the presence of *cis*-[$Mn^{III}Br_{12}$DAPDPP]Cl and PhI(OAc)$_2$, but the system becomes less selective and catalyst destruction augments.

Addition of imidazole (at a MnP/Im ratio of 1:0.5) to the systems based on PhI(OAc)$_2$ (as oxidant) significantly increases Cy-ol in the case of [Mn^{III}TPP]Cl and *cis*-[Mn^{III}DAPDPP]Cl, while product selectivity remains unaltered. This might be due to axial coordination of imidazole to the MnP metal center, which enhances the reactivity of the high-valent active catalytic species. As for the third-generation *cis*-[$Mn^{III}Br_{12}$DAPDPP]Cl, Cy-ol falls significantly, as a result of the steric hindrance conferred by the saddle-shaped conformation of the catalyst.

Comparison of catalyst efficiency in the presence of the oxidants PhI(OAc)$_2$ and PhIO during cyclohexane oxidation with added imidazole shows that the former oxidant gives

rise to more efficient systems. Hence, $PhI(OAc)_2$ is an attractive alternative to PhIO in systems with added imidazole.

Few works have described the use of $PhI(OAc)_2$ in metalloporphyrin-catalyzed oxidation in the presence of additives [16, 41, 44]. Only Silva et al. and Li and Xia have reported increased metalloporphyrin catalyst efficiency in the presence of $PhI(OAc)_2$ and imidazole [16, 41].

3.3.6. MnP-catalyzed cyclohexane oxidation by PhIO or $PhI(OAc)_2$ with addition of water

$[Mn^{III}TPP]Cl$ and *cis*-$[Mn^{III}DAPDPP]Cl$-catalyzed cyclohexane oxidation by PhIO in the presence of 0.5 µL of water (Fig. 7) gives lower product yield when compared with systems without water addition. This result contrasts with the report by Silva et al. [16] and the comparison of the catalysts, *cis*-$[Mn^{III}DAPDPP]Cl$ (with two $–NH_2$ group, Figure 1) and $[Mn^{III}APTPP]Cl$ (with one $–NH_2$ group) from the work by Silva et al. [16], shows that the introduction of only one amino group ($-NH_2$) into the *para-meso*aryl position of the porphyrin ring impacts on the catalytic behavior of this catalysts. These findings suggest that the presence of water may make intermolecular coordination of the amino groups to the metal center more difficult – hydrogen-bonding may occur between the amino group and water, which should decrease product yield and selectivity for Cy-ol. CarvalhoDa-Silva et al. [17] achieved similar results when they used metalloporphyrins bearing ($-COOCH_3$) groups in the *para-meso*aryl positions of the porphyrin macrocycle, which may also form hydrogen bonds with water. Therefore, we decided to verify how addition of larger amounts of water to the systems based on PhIO as oxidant affects product yield (Fig. 7).

Figure 7

Concerning the second-generation *cis*-[Mn^{III}DAPDPP]Cl, addition of 1.0 µL of water increases product yields (Cy-ol + Cy-one) and lowers the degree of catalyst destruction, probably because water coordinates to the metal center. As proposed by Barcells et al. [14], the reactivity of the high-valent catalytic active species increases, which diminishes catalyst destruction by avoiding displacement of the metal ion from the porphyrin macrocycle plane. Regarding the third-generation *cis*-[$Mn^{III}Br_{12}$DAPDPP]Cl, addition of 1.0 µL of water also elevates product yield, but catalyst degradation remains unaffected. Addition of larger amounts of water shows that maximum product yield emerges after addition of 2.5 and 1.0 µL of water to the system based on *cis*-[Mn^{III}DAPDPP]Cl and *cis*-[$Mn^{III}Br_{12}$DAPDPP]Cl, respectively. Interestingly, higher amounts of this ligand slightly reduce product yield, but the yield is still superior to the yield obtained without addition of water.

When $PhI(OAc)_2$ is the oxidant, addition of 0.5 µL of water elicits different changes as compared with PhIO as oxidant. For the second-generation *cis*-[Mn^{III}DAPDPP]Cl, the product (Cy-ol + Cy-one) yield rises, whereas the yield remains virtually the same in the case of the third-generation *cis*-[$Mn^{III}Br_{12}$DAPDPP]Cl. For both *cis*-[Mn^{III}DAPDPP]Cl and *cis*-[$Mn^{III}Br_{12}$DAPDPP]Cl, amounts of water larger than 1.0 µL do not significantly modify product yield, which are always superior to the product yield achieved in the absence of water. Larger yields in the presence of $PhI(OAc)_2$ and water suggest that $PhI(OAc)_2$ hydrolyzes and generates PhIO in situ, as proposed by In et al. [15]. Furthermore, water can also act as an axial ligand, as proposed by Barcells et al. [14]. Together, these two phenomena justify larger product yields in the presence of water and $PhI(OAc)_2$.

4. Conclusion

The brominated third-generation *cis*-[$Mn^{III}Br_{12}$DAPDPP]Cl complex results from direct bromination of *cis*-[Mn^{III}DAPDPP]Cl, which comprises only two steps. This type of bromination reaction meets the requirements of green chemistry, but the scientific

community does not employ it very often [27]. Application of the synthesized second-generation *cis*-[Mn^{III}DAPDPP]Cl and the third-generation *cis*-[$Mn^{III}Br_{12}$DAPDPP]Cl as catalysts for the oxidation of poorly reactive organic substrates by PhIO or $PhI(OAc)_2$ reveals some interesting features. The yield of *n*-hexane oxidation is low, which attests to the high stability of this linear alkane. As for the oxidation of adamantane, a cyclic alkane, both MnPs are regioselective for 1-Adol. Regioselectivity is as high as 100% in the presence of the second-generation *cis*-[Mn^{III}DAPDPP]Cl and $PhI(OAc)_2$. The third-generation *cis*-[$Mn^{III}Br_{12}$DAPDPP]Cl gives large product yields during cyclohexane oxidation by either PhIO or $PhI(OAc)_2$.

Addition of 0.5 µL of water during cyclohexane oxidation by PhIO reduces yields. Larger amounts of water improve product yield in the case of both MnPs, 2.5 and 1.0 µL of water for *cis*-[Mn^{III}DAPDPP]Cl and *cis*-[$Mn^{III}Br_{12}$DAPDPP]Cl, respectively. Further addition of water lowers product yield, which might be a consequence of MnP hexacoordination – this type of coordination saturates the catalyst coordination sphere and makes the MnP unavailable for reaction with the oxidant. The addition of water during cyclohexane oxidation by $PhI(OAc)_2$ increases product yield, especially in the case of *cis*-[Mn^{III}DAPDPP]Cl. However, a more detailed investigation into how water influences organic substrate oxidation is necessary to establish the role that this ligand plays in the reactions.

This work has verified that the third-generation *cis*-[$Mn^{III}Br_{12}$DAPDPP]Cl is a more efficient catalyst than the second-generation *cis*-[Mn^{III}DAPDPP]Cl, irrespective of the oxidant. $PhI(OAc)_2$ can replace PhIO as an oxidant; indeed, sometimes the former oxidant is even more efficient than the latter.

Acknowledgements

Financial support from CNPq, and FAPEMIG is gratefully acknowledged. We are grateful to Prof. Dr. Paulo Jorge Sanches Barbeira for use of the potentiostat Eco Chemie l-Autolab during cyclic voltammetry analysis.

References

[1] B. Meunier, S.P. de Visser, S. Shaik, Chem. Rev. 104 (2004) 3947-3980.

[2] R.A. Periana, G. Bhalla, W.J. Tenn, K.J.H. Young, X.Y. Liu, O. Mironov, C.J. Jones, V.R. Ziatdinov, J. Mol. Catal. A: Chem. 220 (2004) 7-25.

[3] J.T. Groves, T.E. Nemo, R.S. Myers, J. Am. Chem. Soc., 101 (1979) 1032-1033.

[4] B. Meunier, Chem. Rev. 92 (1992) 1411-1456.

[5] C.-M. Che, V.K.-Y. Lo, C.-Y. Zhou, J.-S. Huang, Chem. Soc. Rev. 40 (2011) 1950-1975.

[6] C.-C. Guo, X.-Q. Liu, Q. Liu, Y. Liu, M.-F. Chu, W.-Y. Lin, J. Porphyrins Phthalocyanines. 13 (2009) 1250-1254.

[7] C.L. Hill, B.C. Schardt, J. Am. Chem. Soc., 102 (1980) 6374-6375.

[8] J.A. Smegal, B.C. Schardt, C.L. Hill, J. Am. Chem. Soc.,105 (1983) 3510-3515.

[9] G.R. Friedermann, M. Halma, K.A. Dias de Freitas Castro, F.L. Benedito, F.G. Doro, S.M. Drechsel, A.S. Mangrich, M.d.D. Assis, S. Nakagaki, Appl. Catal A: Gen. 308 (2006) 172-181.

[10] R. Latifi, L. Tahsini, B. Karamzadeh, N. Safari, W. Nam, S.P. de Visser, Arch. Biochem. Biophys. 507 (2011) 4-13.

[11] Z. Solati, M. Hashemi, S. Hashemnia, E. Shahsevani, Z. Karmand, J. Mol. Catal. A: Chem. 374 (2013) 27-31.

[12] K.A. Jorgensen, P. Swanstrom, Acta Chem. Scand. 43 (1989) 822-824.

[13] M.J. Gunter, P. Turner, J. Mol. Catal. 66 (1991) 121-141.

[14] D. Balcells, C. Raynaud, R.H. Crabtree, O. Eisenstein, Inorg. Chem. 47 (2008) 10090-10099.

[15] J.-H. In, S.E. Park, R. Song, W. Nam, Inorg. Chim. Acta. 343 (2003) 373-376.

[16] V.S. da Silva, L.I. Teixeira, E. do Nascimento, Y.M. Idemori, G. DeFreitas-Silva, Appl. Catal A: Gen. 469 (2014) 124-131.

[17] D. da Silva, G. DeFreitas-Silva, E. do Nascimento, J. Reboucas, P. Barbeira, M. de Carvalho, Y. Idemori, J. Inorg. Biochem. 102 (2008) 1932-1941.

[18] T.P. Wijesekera, D.A. Dolphin, in: R.A. Sheldon (Ed.), Metalloporphyrins in Catalytic Oxidations, New York, 1994, pp. 193–239.

[19] H. Saltzman, J.G. Sharefkin, Org. Synth. 43 (1963) 60–61.

[20] G. Gritzner, J. Kuta, Pure Appl. Chem. 56 (1984) 461-466.

[21] E. Hasegawa, J.I. Nemoto, T. Kanayama, E. Tsuchida, Eur. Polymer. J. 14 (1978) 123-127.

[22] A. de Sousa, M. de Carvalho, Y. Idemori, J. Mol. Catal. A: Chem. 169 (2001) 1-10.

[23] M. Ribani, C. Bottoli, C. Collins, I. Jardim, L. Melo, Quim. Nova. 27 (2004) 771-780.

[24] R. Luguya, L. Jaquinod, F.R. Fronczek, A.G.H. Vicente, K.M. Smith, Tetrahedron. 60 (2004) 2757-2763.

[25] F.R. Longo, Finarell.Mg, J.B. Kim, J. Heteroc. Chem. 6 (1969) 927- 931.

[26] L.J. Boucher, J.J. Katz, J. Am. Chem. Soc., 89 (1967) 1340-1345.

[27] J.S. Reboucas, G. DeFreitas-Silva, I. Spasojevic, Y.M. Idemori, L. Benov, I. Batinic-Haberle, Free Radical Biol. Med. 45 (2008) 201-210.

[28] M. Autret, Z.P. Ou, A. Antonini, T. Boschi, P. Tagliatesta, K.M. Kadish, J. Chem. Soc.,Dalton Trans. (1996) 2793-2797.

[29] G. Hariprasad, S. Dahal, B.G. Maiya, J. Chem. Soc. Dalton Trans., (1996) 3429-3436.

[30] P. Bhyrappa, P. Bhavana, Chem. Phys. Lett. 349 (2001) 399-404.

[31] P. Bhyrappa, V. Krishnan, Inorg. Chem. 30 (1991) 239-245.

[32] A. Ghosh, I. Halvorsen, H.J. Nilsen, E. Steene, T. Wondimagegn, R. Lie, E. van Caemelbecke, N. Guo, Z.P. Ou, K.M. Kadish, J. Phys. Chem. B. 105 (2001) 8120-8124.

[33] E. do Nascimento, G.D. Silva, F.A. Caetano, M.A.M. Fernandez, D.C. da Silva, M. de Carvalho, J.M. Pernaut, J.S. Reboucas, Y.M. Idemori, J. Inorg. Biochem. 99 (2005) 1193-1204.

[34] D. Mansuy, Coord. Chem. Rev.. 125 (1993) 129-141.

[35] M. Costas, Coord. Chem. Rev. 255 (2011) 2912-2932.

[36] J.M. Thomas, R. Raja, G. Sankar, R.G. Bell, Nature. 398 (1999) 227-230.

[37] B.R. Cook, T.J. Reinert, K.S. Suslick, J. Am. Chem. Soc., 108 (1986) 7281-7286.

[38] J.A. Kerr, Chem. Rev. 66 (1966) 465-&.

[39] Z. Valicsek, O. Horvath, G. Lendvay, I. Kikas, I. Skoric, J. Photochem. Photobiol. A. 218 (2011) 143-155.

[40] F.G. Doro, J.R.L. Smith, A.G. Ferreira, M.D. Assis, J. Mol. Catal. A: Chem. 164 (2000) 97-108.

[41] Z. Li, C.G. Xia, J. Mol. Catal. A: Chem. 214 (2004) 95-101.

[42] B.R. Santos Lemos, D. CarvalhoDa-Silva, D.Z. Mussi, L.d.S. Santos, M.M. da Silva, M.E. Moreira Dai de Carvalho, J.S. Reboucas, Y.M. Idemori, Appl. Catal A: Gen. 400 (2011) 111-116.

[43] M. Gardner, A.J. Guerin, C.A. Hunter, U. Michelsen, C. Rotger, New J. Chem. 23 (1999) 309-316.

[44] G.d.F. Silva, D.C. da Silva, A.S. Guimaraes, E. do Nascimento, J.S. Reboucas, M.P. de Araujo, M.E. Moreira Dai de Carvalho, Y.M. Idemori, J. Mol. Catal. A: Chem. 266 (2007) 274-283.

Figure Captions

Figure 1. Structural representation of the porphyrin and manganese porphyrin complexes employed in this work.

Figure 2. UV-vis absorption spectra of *cis*-H_2DAPDPP (5.11 x 10^{-6} mol L^{-1}), *cis*-[Mn^{III}DAPDPP]Cl (1.79 x 10^{-5} mol L^{-1}) and *cis*-[$Mn^{III}Br_{12}$DAPDPP]Cl (1.06 x 10^{-5} mol L^{-1}) in CH_2Cl_2.

Figure 3. Structural representation of cyclohexane, *n*-hexane, and adamantane oxidation reactions.

Figure 4. Oxidation of n-hexane by PhIO or $PhI(OAc)_2$ catalyzed by MnP in CH_2Cl_2: 1-hexanol (1-ol), 2-hexanol (2-ol), 3-hexanol (3-ol), 2-hexanone (2-one), and 3-hexanone(3-one) yields and degree of catalyst destruction. Reactions in the absence of catalyst did not yield any significant amount of the products. Reaction conditions: [MnP] = 5 × 10^{-4} mol L^{-1}, [oxidant] = 5 × 10^{-3} mol L^{-1}, MnP/oxidant/n-hexane/CH_2Cl_2 molar ratio = 1:10:3800:15550, 25 ℃, magnetic stirring.

Figure 5. Oxidation of adamantane by PhIO or $PhI(OAc)_2$ catalyzed by MnP in CH_2Cl_2: 1-Adamantanol (1-Adol), 2-Adamantanol (2-Adol), and 2-Adamantanone (2-Adone) yields, regioselectivity toward 1-Adol, and degree of catalyst destruction. Reactions in the absence of catalyst did not yield any significant amount of the products. Reaction conditions: [MnP] = 5 × 10^{-4} mol L^{-1}, [oxidant] = 5 × 10^{-3} mol L^{-1}, MnP/oxidant/adamantane/CH_2Cl_2 molar ratio = 1:10:100:15550, 25 ℃, magnetic stirring. Regioselectivity for 1-Adol [=100%. 1-Adol /(1-Adol + (2-Adol + 2-Adone)/3)].

Figure 6. Cyclohexanol (Cy-ol) and cyclohexanone (Cy-one) yields and selectivity toward cyclohexanol obtained in the oxidation of cyclohexane by PhIO, PhIO in the presence of imidazole, $PhI(OAc)_2$, and $PhI(OAc)_2$ in the presence of imidazole, catalyzed by MnP in CH_2Cl_2. Reactions in the absence of catalyst did not yield any significant amount of the products. Reaction conditions: [MnP] = 5×10^{-4} mol L^{-1}, [oxidant] = 5×10^{-3} mol L^{-1}, MnP/oxidant/cyclohexane/CH_2Cl_2 molar ratio = 1:10:4650:15550, 25 ℃, magnetic stirring. Selectiv ity Cy-ol [=100%. Cy-ol/(Cy-ol + Cy-one)].

Figure 7. Oxidation of cyclohexane by PhIO or $PhI(OAc)_2$ catalyzed by MnP in CH_2Cl_2: cyclohexanol (Cy-ol) and cyclohexanone (Cy-one) yields, selectivity toward cyclohexanol, and degree of catalyst destruction. Reactions in the absence of catalyst did not yield any significant amount of the products. Reaction conditions: [$Mn^{III}P$] = 5×10^{-4} mol L^{-1}, [oxidant] = 5×10^{-3} mol L^{-1}, MnP/oxidant/cyclohexane/CH_2Cl_2 molar ratio = 1:10:4650:15550, 25 ℃, magnetic stirring. Selectiv ity Cy-ol [=100%. Cy-ol/(Cy-ol + Cy-one)].

Table 1. Potentials of the anodic peak (E_{pa}) and cathodic peak (E_{pc}) and of the half-wave potential ($E_{1/2}$) vs Fc^+/Fc for Mn^{III}/Mn^{II} in manganese porphyrins (in CH_2Cl_2, $TBABF_4$ 0.1 mol L^{-1}, 100 mV s^{-1}).

Complex	E_{pa} (mV)	E_{pc} (mV)	$E_{1/2}$ (mV)	$\Delta E_{1/2}$ (mV)
cis-[Mn^{III}DAPDPP]Cl	- 765	- 892	- 829	-
cis-[$Mn^{III}Br_{12}$DAPDPP]Cl	- 273	- 373	- 323	506

Figure

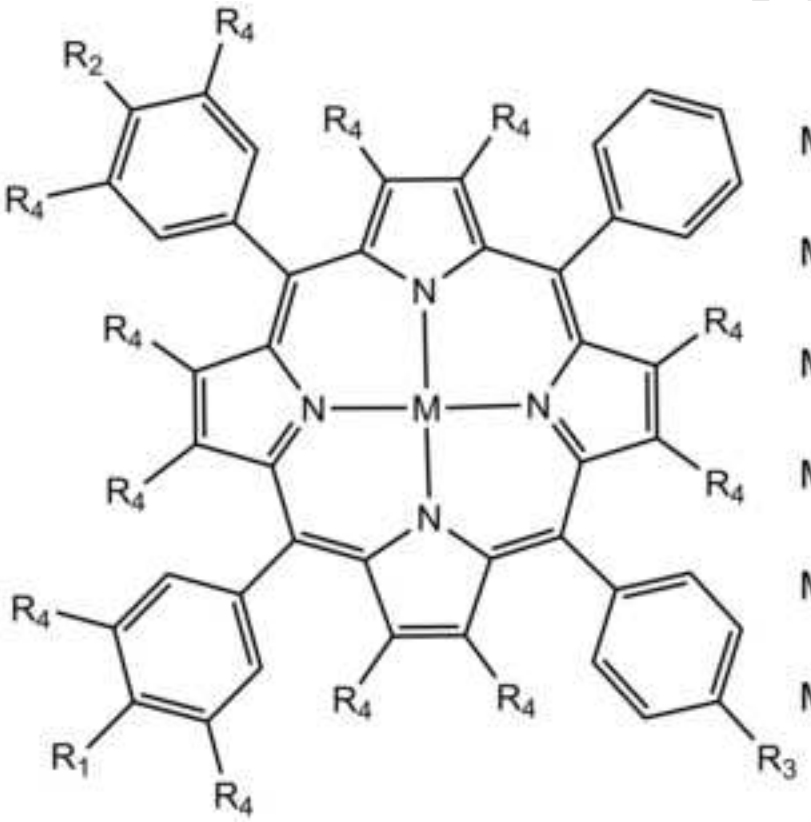

M = 2H; R_1, R_2 = NO_2; R_3, R_4 = H: cis-H_2DNPDPP

M = 2H; R_2, R_3 = NO_2; R_1, R_4 = H: trans-H_2DNPDPP

M = 2H; R_1, R_2 = NH_2; R_3, R_4 = H: cis-H_2DAPDPP

M = 2H; R_2, R_3 = NH_2; R_1, R_4 = H: trans-H_2DAPDPP

M = Mn; R_1, R_2 = NH_2; R_3, R_4 = H: cis-[Mn^{III}DAPDPP]Cl

M = Mn; R_1, R_2 = NH_2; R_3= H, R_4 = Br: cis-[$Mn^{III}Br_{12}$DAPDPP]Cl

Figure

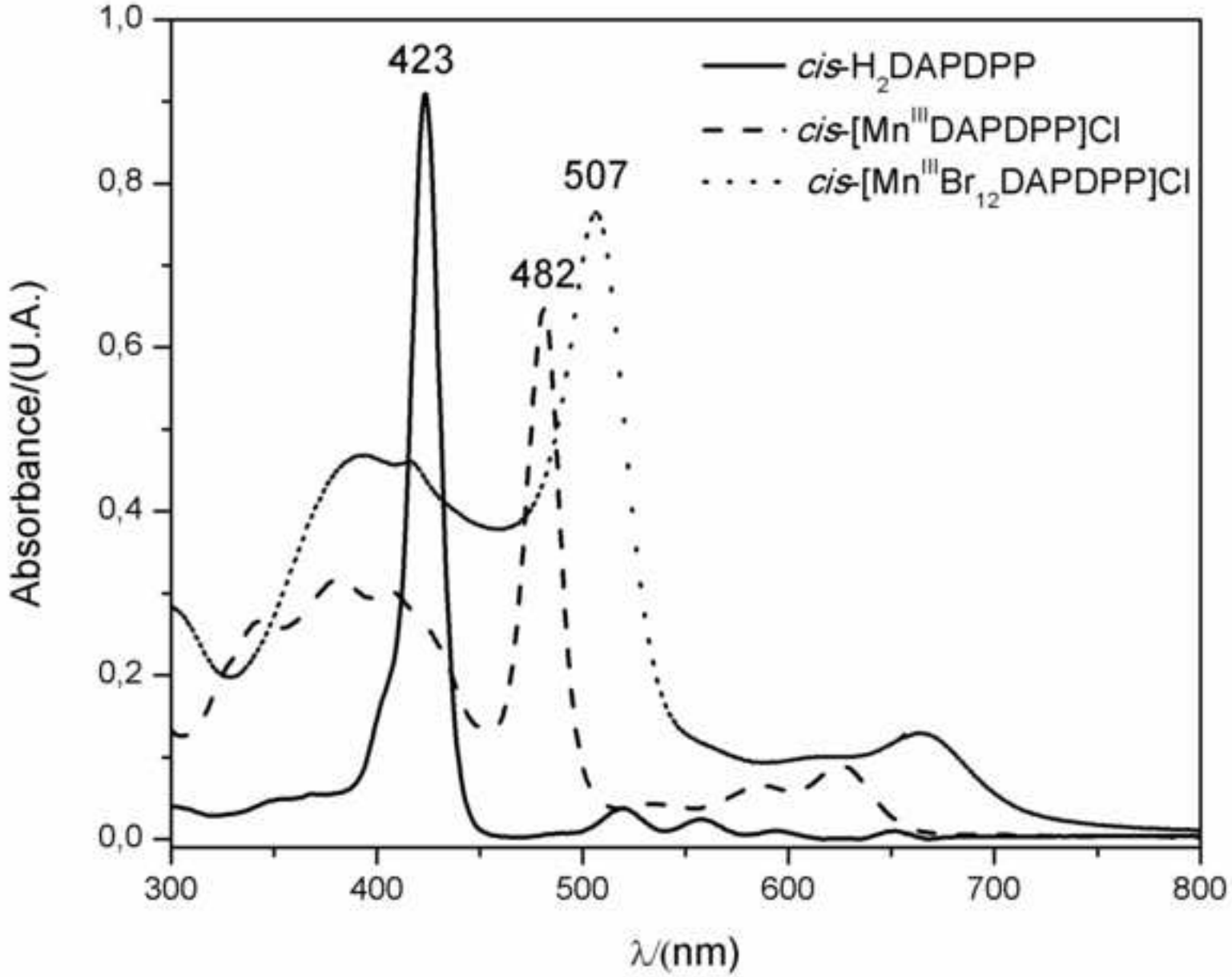
1,0
0,8
0,6
0,4
0,2
0,0
Absorbance/(U.A.)
300
400
500
600
700
800
λ/(nm)
423
507
482
cis-H2DAPDPP
cis-[MnIIIDAPDPP]Cl
cis-[MnIIIBr12DAPDPP]Cl

Figure

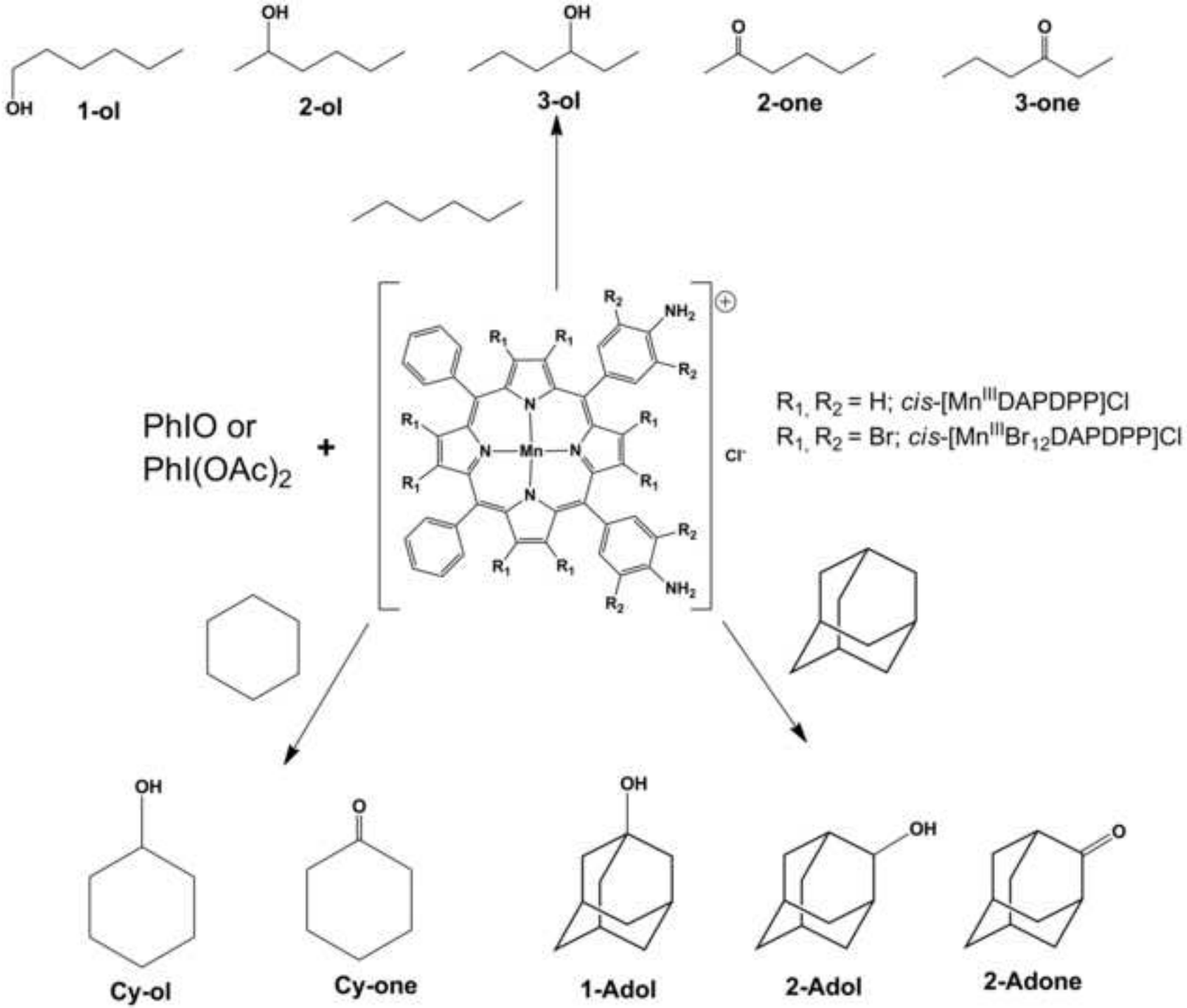
1-ol
2-ol
3-ol
2-one
3-one
PhIO or
PhI(OAc)2
+
Cl-
R1, R2 = H; cis-[MnIIIDAPDPP]Cl
R1, R2 = Br; cis-[MnIIIBr12DAPDPP]Cl
Cy-ol
Cy-one
1-Adol
2-Adol
2-Adone

Figure

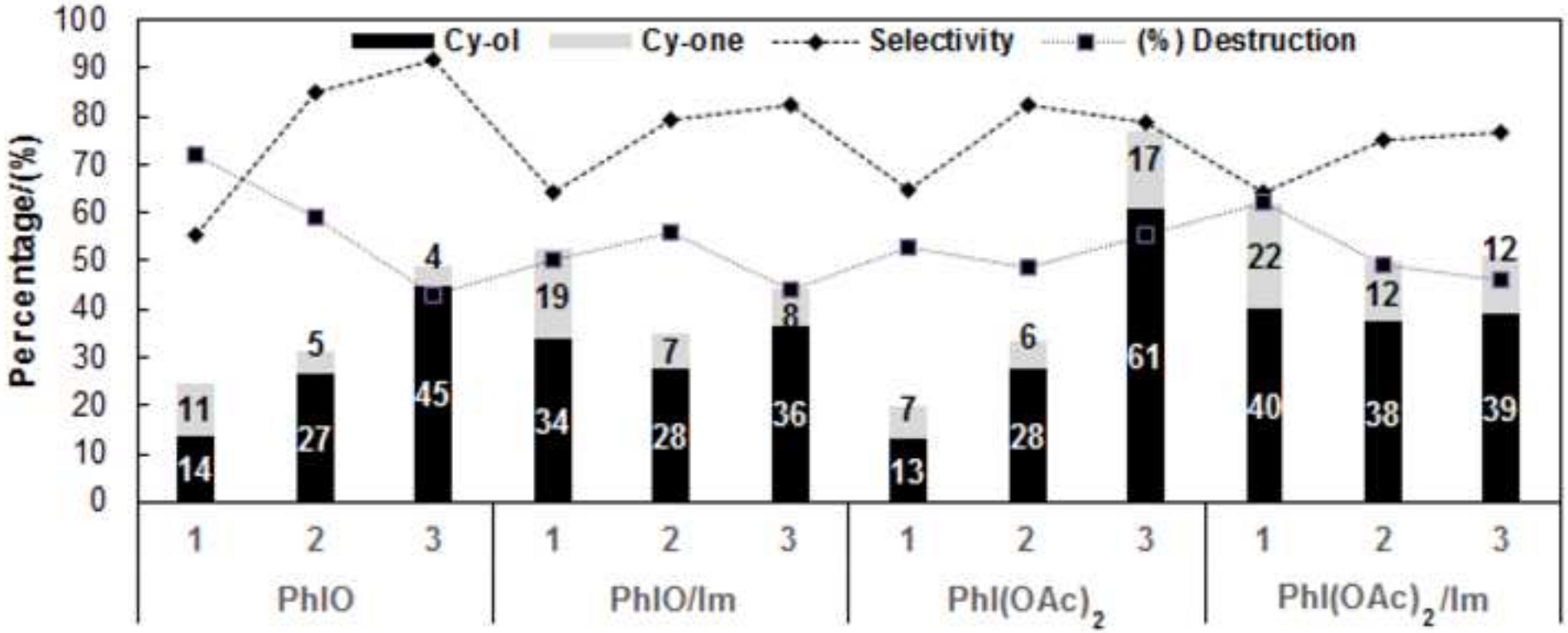
Cy-ol
Cy-one
Selectivity
(%) Destruction
Percentage/(%)
100
90
80
70
60
50
40
30
20
10
0
14
11
27
5
45
4
34
19
28
7
36
8
13
7
28
6
61
17
40
22
38
12
39
12
1
2
3
PhIO
PhIO/Im
PhI(OAc)2
PhI(OAc)2/Im

Figure

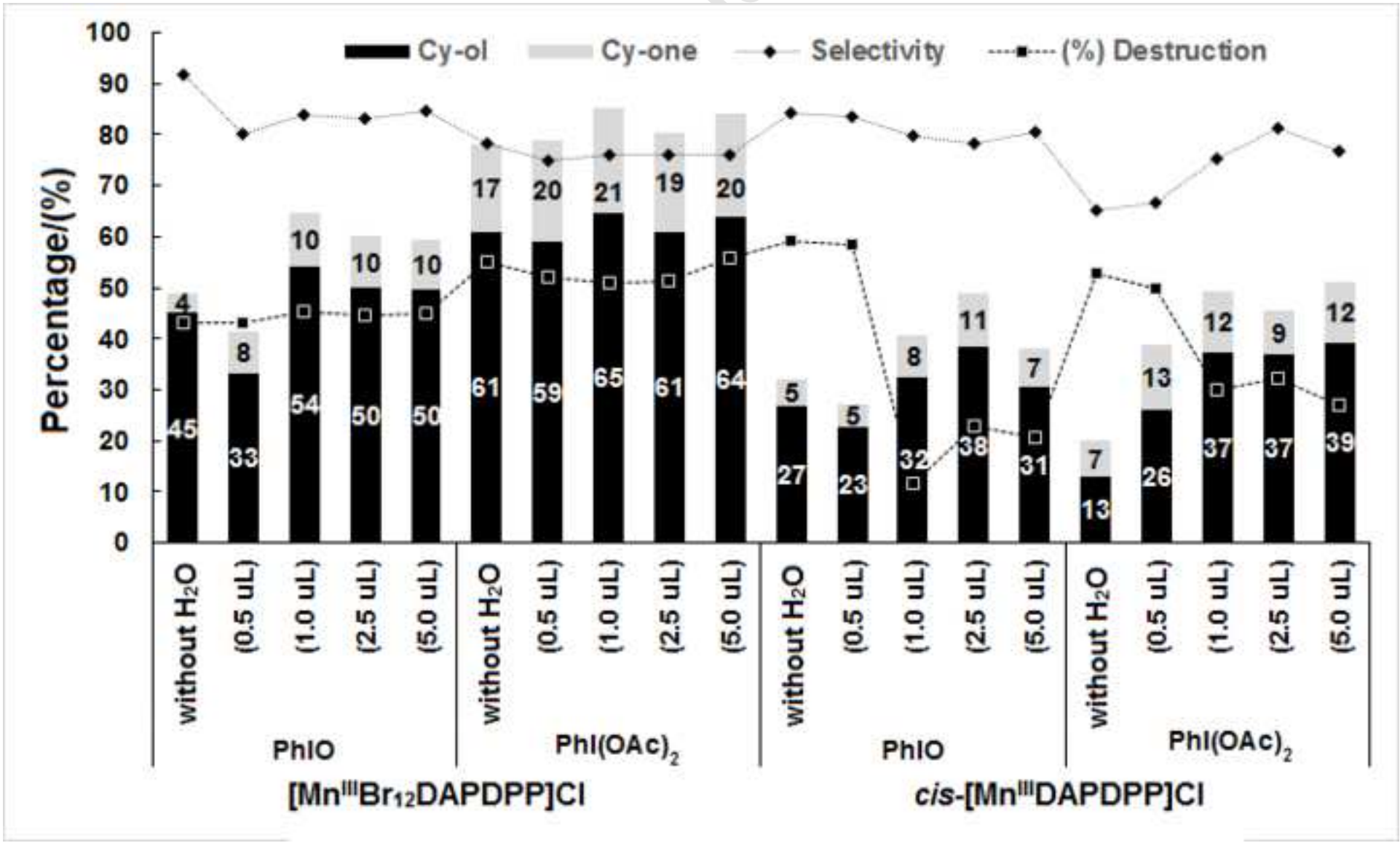
Cy-ol
Cy-one
Selectivity
(%) Destruction
Percentage/(%)
100
90
80
70
60
50
40
30
20
10
0
without H2O
(0.5 uL)
(1.0 uL)
(2.5 uL)
(5.0 uL)
PhIO
PhI(OAc)2
[MnIIIBr12DAPDPP]Cl
cis-[MnIIIDAPDPP]Cl

Figure

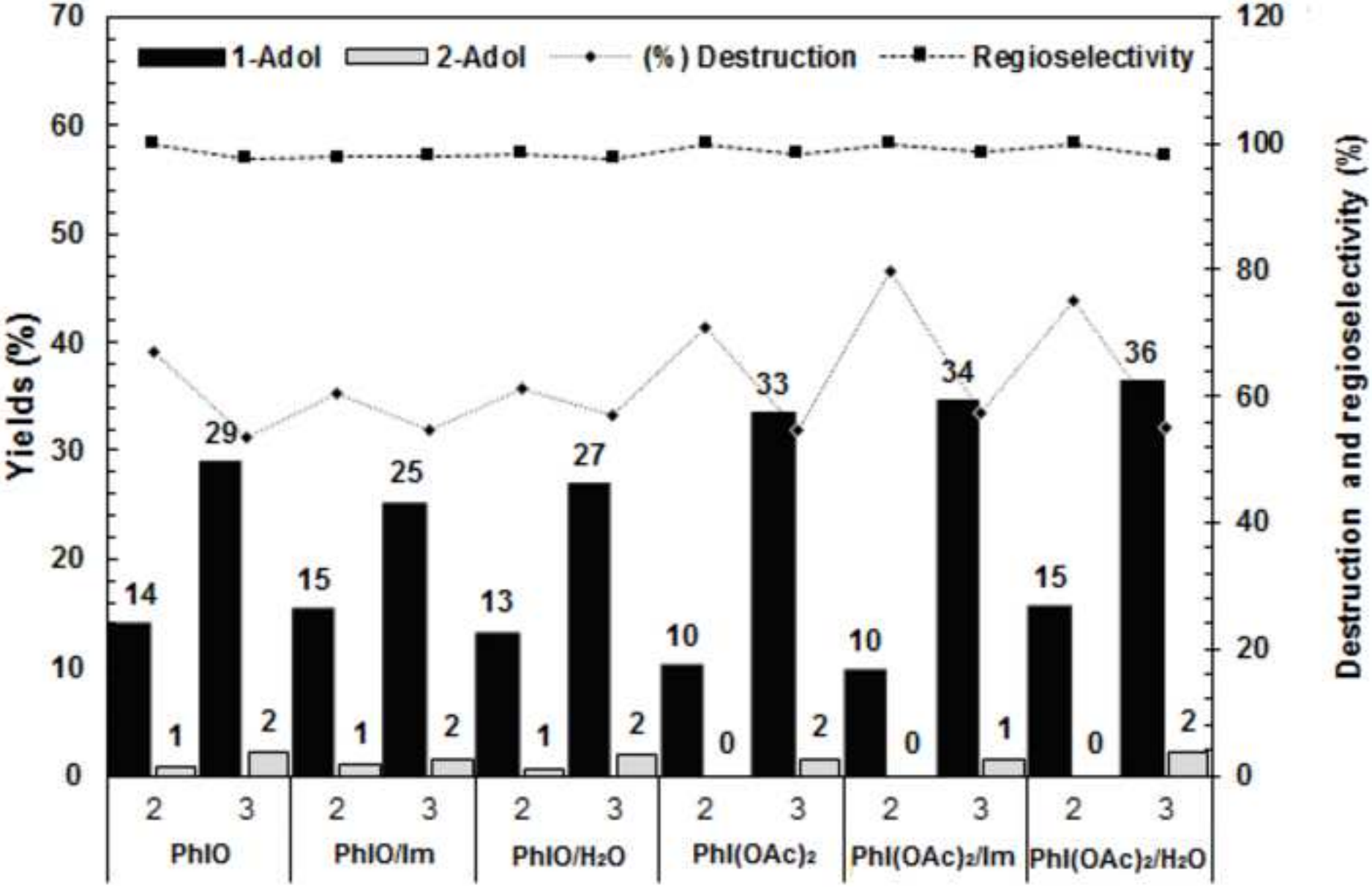
1-Adol
2-Adol
(%) Destruction
Regioselectivity
Yields (%)
Destruction and regioselectivity (%)
70
60
50
40
30
20
10
0
120
100
80
60
40
20
0
14
1
29
2
15
1
25
2
13
1
27
2
10
0
33
2
10
0
34
1
15
0
36
2
2
3
PhIO
PhIO/Im
PhIO/H2O
PhI(OAc)2
PhI(OAc)2/Im
PhI(OAc)2/H2O

Figure

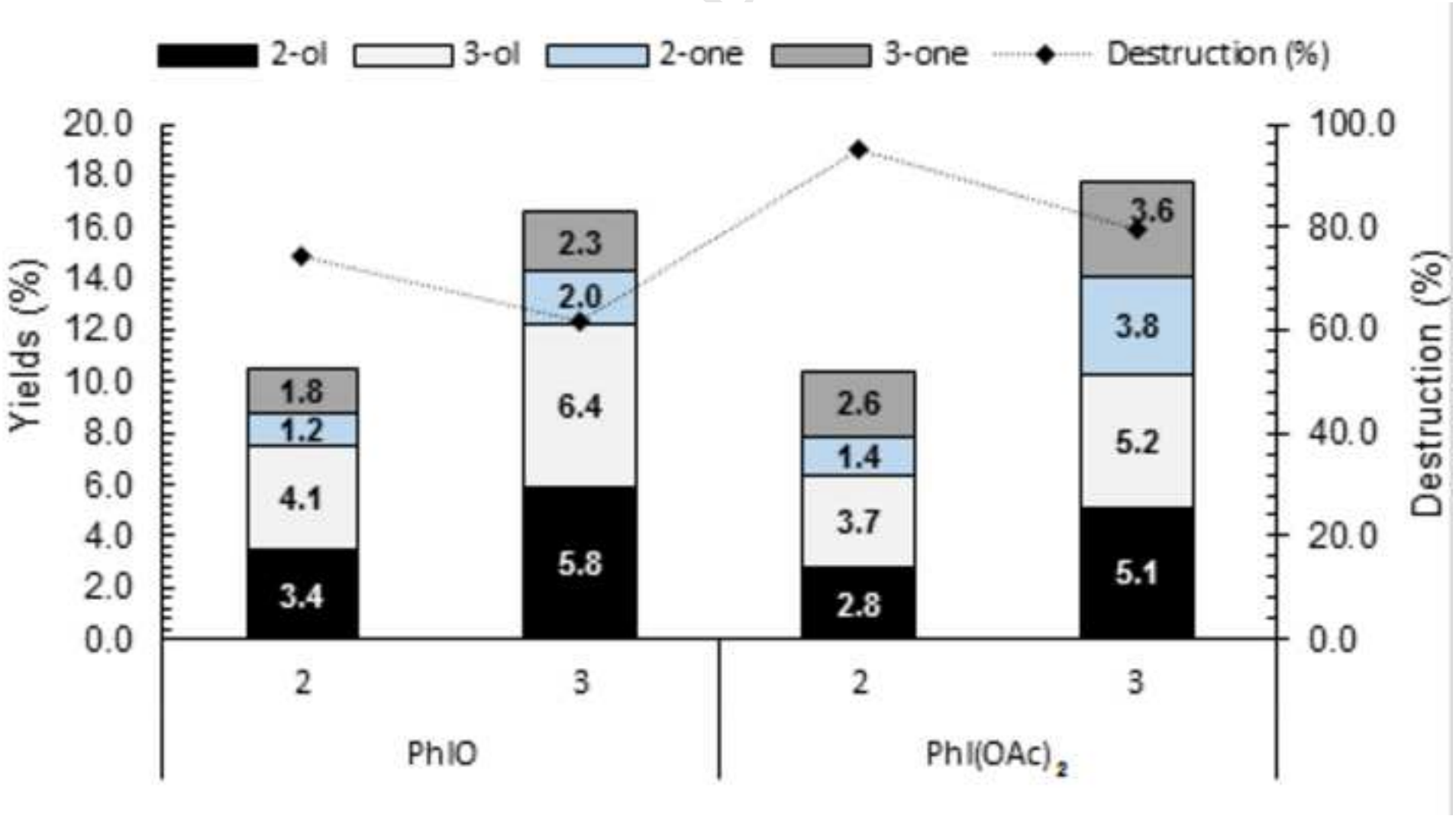
2-ol
3-ol
2-one
3-one
Destruction (%)
Yields (%)
Destruction (%)
20.0
18.0
16.0
14.0
12.0
10.0
8.0
6.0
4.0
2.0
0.0
100.0
80.0
60.0
40.0
20.0
0.0
1.8
1.2
4.1
3.4
2.3
2.0
6.4
5.8
2.6
1.4
3.7
2.8
3.6
3.8
5.2
5.1
2
3
2
3
PhIO
PhI(OAc)2